The Spatial Organisation of Time-averaged Streamwise Velocity and its Correlation with the Surface Topography of Water-worked Gravel Beds

James R. Cooper[1] and Simon J. Tait[2]

[1] Department of Geography, University of Hull, Cottingham Road, Hull, HU6 7RX, UK. email: j.r.cooper@hull.ac.uk
[2] School of Engineering, Design and Technology, University of Bradford, Richmond Road, Bradford, BD7 1DP, UK.

Abstract

An examination was made into the spatial pattern of time-averaged streamwise velocity in the near-bed region over two water-worked gravel beds. Laboratory observations revealed that there is considerable spatial variability in velocity. It was organised into streamwise streaks of high-speed fluid which were overlain by spots of low-speed fluid. This spatial pattern was found to be consistently and heavily dependent on relative submergence. The spatial pattern of velocity was shown to have little linear coherence with bed surface topography at the grain-scale. It suggested that for flows above the two beds studied here, bed surface topography at the grain-scale exerted less of an influence on the spatial organisation of time-averaged streamwise velocities than relative submergence.

Key words: velocity, spatial organisation, bed surface topography, water-worked gravel beds, laboratory flume.

1. INTRODUCTION

The surface of a water-worked gravel bed displays a spatially complex, three-dimensional, structure. Any study of the interaction between the fluid and such a bed must be able to examine the relationship between this structure and the spatial characteristics of the turbulent flow. Several studies have made qualitative assessments of the effects of bed surface topography on time-averaged streamwise velocity, describing it in terms of the influence of isolated roughness elements (Clifford, 1996; Lane et al., 2002; Papanicolaou and Hilldale, 2002; Lane et al., 2004; Tritico and Hotchkiss, 2005), pebble clusters (Buffin-Bélanger and Roy, 1998; Lawless and Robert, 2001), or in the form of secondary currents (McLelland et al., 1999; Carling et al., 2002; Papanicolaou and Hilldale, 2002). The majority of these studies have examined the flow over beds with well defined large clasts or large pebble clusters, or within a single cross-section or transect of a channel, rather than over a representative section of bed.

More recently, attempts have been made to assess the effect of a distribution of roughness elements on the spatial variability in time-averaged streamwise velocity at the reach scale. Lamarre and Roy (2005) collected a more spatially detailed field data set of velocity and bed surface topography measurements. Their examination of the effect of bed surface topography on time-averaged streamwise velocity still remained qualitative and focussed on the effects of individual roughness elements on the shape of the vertical velocity profile. Legleiter et al. (2007) were the first to attempt to relate quantitatively the spatial patterns in the time-averaged streamwise velocity to bed roughness. They carried out velocity measurements along five lateral cross-sections within a cobble-bedded river at three different discharges. The magnitude of the correlation between bed roughness and time-

averaged streamwise velocity was shown to be relatively weak at all three discharges, with values of the coefficient of correlation in the range of around –0.5 to 0.5. The correlation was based on using depth-averaged velocity values not near-bed values, so it is unclear whether this may have caused the weak correlation between bed roughness and time-averaged streamwise velocity. By comparing cross-correlograms between bed roughness and time-averaged streamwise velocity, they also discovered that there was a stage-dependent effect of local boundary roughness on the time-averaged flow. The strength of the correlation between time-averaged streamwise velocity and bed roughness increased with flow depth, suggesting that the flow became more spatially coherent as stage increased. They stated that the results demonstrated that the flow field at the small-scale was influenced by topographic variability at high spatial frequencies, most noticeably at lower depths, and that the overall large-scale flow pattern primarily reflected the bulk morphology of the channel. This influence was said to change with flow depth, such that the localised influence of bed surface topography was increasingly smoothed out as flow depth increased. They suggested that this was due to the effects of the bed surface topography diminishing at higher flow depths as well-defined secondary currents developed in response to the more salient topographic features of the channel. From this, they concluded that the flow primarily responds to the gross morphology of the channel and that flow depth is the primary control on flow structure. But the low spatial resolution of velocity and bed elevation measurements within the reach meant that the effects of bed roughness on the flow could only be tentatively determined. Several other studies have reported on the influence of relative submergence on the spatial variability in time-averaged streamwise velocities (Clifford, 1996; Lawless and Robert, 2001), however it still remains unclear how relative submergence influences the spatial organisation of time-averaged streamwise velocity.

The lack of data sets of detailed bed surface topography measurements combined with high spatial resolution velocity measurements explains why spatial variability has often been examined in terms of the effects of individual roughness elements. No study has been able to examine the influence of the microtopography of water-worked gravel beds on the spatial organisation in the time-averaged flow in a detailed, quantitative manner and over a number of different relative submergences.

In this paper, we present detailed, high spatial resolution measurements of time-averaged streamwise velocity and bed surface topography at the grain-scale over two water-worked gravel beds in a laboratory flume. This is performed for a number of hydraulic conditions in which the relative submergence is changed. The objectives are (1) to describe the spatial organisation of time-averaged streamwise velocity and how it is influenced by relative submergence and (2) to assess quantitatively the relationship between the spatial organisation of time-averaged streamwise velocity and bed surface topography at the grain-scale.

2. METHODOLOGY

Experimental Programme

All the experiments were carried out in a 18.3 m long, 0.5 m wide, recirculating, glass-sided flume, with a working length of 15 m. The channel slope was adjustable via the use of a hydraulic jack. The bed and water surface measurements were made relative to a datum plane, defined by two rails parallel with the flume bed. The distance from this

datum plane to the bed surface and the water surface was measured using vernier point gauges. The flow rate was monitored using a pre-calibrated orifice plate in the upstream delivery pipe.

Two different sediment mixtures were used: a log-normal, unimodal grain-size distribution and a slightly bimodal grain-size distribution (Figure 1). The former consisted of 100 % gravel quarried from alluvial deposits. The grains were not crushed and had the rounded properties of grains found in gravel-bed rivers. The bimodal mixture contained 75 % of the same gravel and 25 % sand obtained from the same deposits. The two mixtures were designed to produce similar values of D_{50}, the grain size at which 50 % of the bed material is finer.

The aim of the experimental programme was to produce a range of hydraulic conditions so that the effects of relative submergence and bed surface topography on the spatial organisation of time-averaged streamwise velocity could be systematically investigated. A total of 22 experimental runs were carried out (Tables 1 and 2). The selected flow conditions were below those required for bed movement so the bed surface topography did not change during each test. For each experimental run, a steady flowrate was introduced and the downstream weir adjusted to achieve uniform depth for as large a reach as possible. The experimental runs were divided into two phases. The first phase of the tests was designed to investigate the effect of a change in relative submergence at a single bed slope (Runs 1-6 and 12-16 in Tables 1 and 2, respectively). Different flow depths d were created using different flow discharges. In the second phase, experimental runs were carried out that used a combination of different flow discharges and bed slopes, so that the mean bed shear stress was almost identical for each run (Runs 6-11 and 16-22 in Tables 1 and 2, respectively). These tests revealed the effects of relative submergence, but under conditions where the average momentum transfer rate at the bed was similar. The runs for the bimodal bed were designed so that the relative submergence d/k and bed slope were approximately the same as for the unimodal bed, where k is the thickness of the interfacial sublayer which is equal to the range in bed surface elevations. This allowed runs to be compared directly. Therefore slightly different flow depths were used between the two beds to account for the difference in k.

Velocity Measurements

A 2-D Dantec Particle Image Velocimetry (PIV) system provided detailed spatial measurements of velocity over the deposits. This system consisted of a New Wave Research Minilase-III double pulsed Nd:YAG laser which operated at a wavelength of 532 nm and a pulse energy level of 50 mJ. It was operated at 9 Hz, and this allowed 5 and a half minutes of the flow to be sampled. A Kodak Megaplus ES1.0 digital camera was used to image the seeding particles.

Many previous studies approaches have taken PIV measurements at one lateral position across the bed (usually the centreline of the flume) by using a vertical light sheet oriented normal to the bed surface, in order to obtain streamwise and vertical velocities (e.g. Tait *et al.*, 1996; Campbell *et al.*, 2005; Sambrook Smith and Nicholas, 2005). In addition, these previous measurements have been taken for a limited number of hydraulic and bed conditions, and in some cases only for one flow depth and slope or over a single rough bed (e.g. Campbell *et al.*, 2005; Sambrook Smith and Nicholas, 2005). One study has attempted a different approach to studying such flows. Barison *et al.* (2003) carried out

PIV measurements above an armouring gravel bed with the light sheet located parallel to the bed surface and with the camera normal to the light sheet. This allowed streamwise and lateral velocities to be measured over a large section of the bed and at many more measurement locations than is possible with the use of PIV in a vertical plane.

This study used the approach of Barison *et al.* (2003), in order to measure streamwise velocities at different streamwise and lateral positions, but at one vertical height above the bed (Figure 2). The camera imaged a measurement area at 9.1 m from the inlet. A glass plate was very lightly positioned on the water surface to ensure there were no distortion from the rippled water surface. Measurements were not taken closer than 10 mm to the glass plate to ensure that these effects did not strongly influence the PIV measurements. This was based on previous analysis of PIV measurements taken in a vertical plane with and without the glass plate.

For each experimental run, measurements were taken at four different heights close to the bed, and above this, further measurements were approximately exponentially distributed within the flow depth. Given that the light sheet had a thickness of approximately 2 mm, no measurements were taken closer than 2.75 mm to the maximum bed elevation, to ensure that there was no interference between the light sheet and the bed surface. Many previous PIV studies have used image areas which could be considered too small to sample fully the spatial variability in the flow. For example, Campbell *et al.* (2005) only examined an area of 61×67 mm over a gravel bed, which was sufficient for investigating the role of individual topographic features on the flow, but may not have fully represented the degree of spatial variability in the time-averaged flow. A larger measurement area of 198.4×200.0 mm was therefore used here.

Once the raw PIV images were collected, they were processed using Dantec's FlowManager software to generate velocity vectors fields using a cross-correlation technique. The images were divided into small rectangular interrogation areas and for each of these areas the images from the first and second pulse were cross-correlated. A moving-average validation was chosen to validate, reject and substitute vectors. In strongly 2-D flow this method has been found to be robust (Westerweel, 1994). More details on the image processing routines can be found in Cooper (2006). An interrogation area of 32×32 pixels was used in the cross-correlation of the images and was chosen as a compromise between spatial resolution and measurement confidence. This corresponded to an area of 6.30×6.30 mm. A time separation between the two light sheet pulses of 1000 μs was chosen to ensure that particle displacements were highly unlikely to be larger than a 1/4 of the length of this interrogation area, which can cause zero-velocity biasing. The interrogation areas were overlapped in both the streamwise and lateral direction to increase the probability that particles near the edges of an interrogation area contributed to the velocity calculation. This provided 61 velocity measurements in each lateral direction and 62 measurements in each streamwise direction, and resulted in 3782 measurements within the image area. It resulted in a separation distance of 3.15 mm between each velocity vector measurement (in both the streamwise and lateral direction). The spatial resolution of the velocity measurements is equal to the length of the interrogation area. This gives a spatial resolution of 6.30 mm, and allows the flow field to be measured at the grain-scale. This means that the PIV measurements were able to resolve large-scale structural features rather than those with dimensions of the Taylor's microscale, which is generally the case in PIV (Dantec, 2000).

For each horizontal PIV plane, the measurements were used to derive time-averaged streamwise velocity $\bar{u}$ for each of the measurement locations over the bed. The spatial variability in $\bar{u}$ was analysed by using the concept of double-averaging methodology, in which the time-averaging of the flow field was supplemented with spatial area averaging in the PIV plane (Nikora *et al.*, 2001). This enabled the double-averaged streamwise velocity $\langle \bar{u} \rangle$ to be calculated at a given height above the bed. To account for the effects of increasing relative submergence, $\bar{u}$ was scaled by $\langle \bar{u} \rangle$. This analysis was only performed for the PIV measurements taken closest to the bed surface at $z/k = 0.20$ over the two beds, where z is the height above the maximum bed elevation. This level is used because this is where any correlation between the near-bed flow and the bed surface is likely to be at its strongest. Consideration was given as to whether to compare the spatial organisation of $\bar{u}/\langle \bar{u} \rangle$ for the different experimental runs at the same values of z/d. However, the measurements taken at $z/k = 0.20$ all fall within the form-induced sublayer (Cooper, 2006), and therefore it was deemed appropriate to compare them at $z/k = 0.20$.

Bed production

Representative natural water-worked surfaces were considered important in order to produce flow fields that exhibit spatial patterns that can be considered as analogous to those found in gravel-bed rivers. Recently, Barison *et al.* (2003) discovered that the near-bed spatial distribution of time-averaged streamwise velocity over gravel beds was significantly different over screeded beds than that over a water-worked bed. Initially over the screeded bed, the distributions were highly positively skewed, with a low proportion of smaller velocities. As the bed surface became more water-worked the flow velocity distributions became flatter, wider and less skewed. This indicated that the way in which the beds are formed might have an important effect on the flow field.

The method of bed production chosen for this study was based on the concept developed to form beds in laboratory flumes to study downstream fining (Paola *et al.*, 1992; Seal *et al.*, 1997; Toro-Escobar *et al.*, 2000), whereby sediment is fed into a running flume to form a sediment deposit. A conveyor belt was used in this study to inject gravel into the flow at twice its transport capacity in order to form a deposit between upstream and downstream fixed bed sections. A flume slope of 0.0055 and a constant discharge of 0.0295 m^3/s were selected for the formation of both beds so that the time-scale was long enough to allow a progressive formation of the bed, but short enough for the bed to form within a reasonable time. Further details on how the beds were formed can be found in Cooper (2006). Feeding was halted when the bed slope remained steady over a period of three hours. This was taken to indicate conditions of equilibrium, where feed rate was equal to bedload transport rate. The resulting deposits adopted a bed slope of 0.00225 and 0.00224 (relative to a channel slope of zero), which are remarkably similar, reflecting the repeatability of the bed production approach. Feeding produced rough, water-worked surfaces, but which were still relatively flat (at the macroscopic scale). It can be suggested that the fed beds formed here represent more faithfully the bed conditions (and therefore flow fields) found in gravel-bed rivers, than mechanically screeded beds.

Bed Surface Topography

The bed surface topography was measured from an orthogonal grid of bed surface elevation measurements. The elevation of each point was measured using a Keyence LC-

5

2450 laser displacement sensor. This was moved over the bed surface in a pre-determined grid of measurement points by an automated positioning system located on the flume rails. The laser displacement sensor could measure to a resolution of 0.5 µm in the vertical, with each measurement being integrated over an area of 20×45 µm. The sensor had a valid vertical measurement range of ±8 mm. Given the range of the grain-size distribution of the sediment mixtures used to produce the beds (Figure 1), the vast majority of the elevation measurements were within this range. However, due to occasional large variations in bed elevation and the slope of the bed, a small number of out of range values were recorded. The worst data set contained 0.1 % out of range readings, while it was typically 0.08 %. None of these readings were elevations that were too large, but rather being too low, meaning that the estimations of maximum bed elevation were not affected. Each out of scale reading was replaced by the average elevation of the adjacent points of the grid of data. The same procedure was applied for any missing data points. Given the low percentage of outliers and missing data points, these corrections can be assumed not to have altered significantly the results drawn from the topography measurements.

Bed surface topography was measured over a 250×250 mm area of the bed at a spacing of 1 mm in both the streamwise and lateral directions. The measurement area was centred on the flume centreline. This was positioned to measure the bed surface topography over which the PIV measurements were taken, so that the measurement positions of the velocity vectors and the bed surface elevations exactly corresponded. An area of 250×250 mm was chosen, rather than an area of 198.4×200 mm, which was the size of the horizontal plane used for PIV measurements. This was so that a range of streamwise and lateral lags could be applied to take into account the downstream and lateral propagation of the flow relative to the bed when examining the correlation between the flow and bed surface topography. The resolution of the sensor and the measurement grid was believed to be capable of describing the features of the bed surface arrangement at a grain scale and therefore when combined with the PIV measurements, allows a high spatial resolution study of the interaction between the bed and the flow at the grain-scale.

3. RESULTS

Spatial Organisation of Time-averaged Streamwise Velocity over the Bed

Variability with Relative Submergence at a Single Bed Slope

Contour plots were produced of $\overline{u}/\langle\overline{u}\rangle$ to illustrate the spatial variability in $\overline{u}$ over the bed. This was to enable comparisons to be made between each of the experimental runs, and so that the relative size of the variability could easily be assessed. These plots allow a visual examination of the size of the spatial variations in $\overline{u}$ between different positions over the bed. Contour plots of $\overline{u}/\langle\overline{u}\rangle$ over the unimodal bed for the runs performed at a single bed slope are shown in Figure 3. It is apparent that the spatial pattern is different between the six plots and appears to be associated with changes in relative submergence d/k. At the lowest relative submergence of 1.2, there is a large area of flow that is, on average, moving faster than $\langle\overline{u}\rangle$ (Figure 3a). Surrounding the large high-speed area is a region of slower fluid. With an increase in relative submergence to 1.9 (Figure 3b), there are now four distinct areas of high-speed streamwise velocity 'streaks', which appear to resemblance the areas of faster fluid seen at a relative submergence of 1.2. These streaks alternate with thin streamwise streaks of slightly slower than average fluid. Overlain on

this pattern are small, discrete areas experiencing slower than average flow, quite often approaching only 70 % of $\langle \overline{u} \rangle$, and there is some evidence of these areas in the previous plot. At a relative submergence of 2.6 the spatial pattern of $\overline{u}/\langle \overline{u} \rangle$ is very similar to that in Figure 3b, with all the high-speed streaks and low-speed spots all occurring in the same locations (Figure 3c). The intensity of some of the low speed-spots has decreased, and a small number of the spots have merged with neighbouring spots. With a further increase in relative submergence to 3.2, the distinction of the high-speed streaks decreases quite markedly (Figure 3d), although all four streaks observed at a relative submergence of 1.9 and 2.6 are still present, displaying some degree of spatial persistence also with those in Figure 3a. The streaks have also grown in lateral extent. Again, the low-speed spots are occurring at the same locations as seen in the previous plots, and the intensity of the spots has decreased. At a relative submergence of 4.1, there is a further reduction in the spatial organisation, with an almost complete disappearance of the high-speed streaks (Figure 3e). There are still some low-speed spots, but they are less distinct and larger in spatial coverage. Furthermore, only a small number of the spots correspond to those seen previously, especially given that a small number of new spots have appeared. A further increase in relative submergence to 5.9 results in the occurrence of two streamwise streaks of higher and lower speed fluid much larger than seen at the lower submergences (Figure 3f), and there is even less correspondence in the locations of the low-speed spots to the previous plots.

Over the bimodal bed, the change in the spatial pattern of $\overline{u}/\langle \overline{u} \rangle$ with relative submergence at a single bed slope can be seen in Figure 4. At the lowest submergence of 1.3 there is no clear structuring of the flow, except in the form of discrete areas of fluid that are flowing both slower and faster than $\langle \overline{u} \rangle$ (Figure 4a). The low-speed spots have a similar intensity and size to those seen at the same relative submergence over the unimodal bed, but there was no evidence of high-speed spots over the unimodal bed. However at a relative submergence of 2.0 it is striking that a similar pattern of high-speed streaks and thinner streaks of lower velocity are also noticeable over the bimodal bed (Figure 4b), as was observed over the unimodal bed. These streaks occupy the whole streamwise length of the bed. Again, overlain on these streaks are low-speed spots. The pattern is more speckled than that over the unimodal bed, suggesting that some of the flow features over the bimodal bed are smaller and more localised. At a relative submergence of 2.7 the same alternating pattern of high- and low-speed streaks is observed (Figure 4c), but it is more distinct than in the previous plot, particularly in the case of the streaks of slower fluid. It is therefore even more comparable to the spatial pattern seen over the unimodal bed at the same relative submergence. The streaks and low-speed spots are all located in almost exactly the same position as seen in the previous plot. An increase in relative submergence to 3.3 results in the disappearance of one of the high velocity streaks in the lower half of the bed through the amalgamation of two streaks (Figure 4d). But the location of the remaining high-speed streaks is remarkably similar to those at a relative submergence of 2.7. Indeed, this also applies to the low-speed spots, with all the spots seen in the previous plot also present. At a relative submergence of 4.3, still only two high-speed streaks remain, but the lower speed streak has become less defined (Figure 4e). The opposite has occurred for the upper most high-speed streak. There are still low-speed spots present, but they are slightly fewer in number. A further increase in relative submergence to 6.2 results in the total disappearance of the streaks of both high- and low-speed fluid (Figure 4f).

The contour plots of $\bar{u}/\langle\bar{u}\rangle$ in Figure 5 again show how the spatial pattern of the near-bed flow changes with relative submergence over the unimodal bed, but this time when the mean bed shear stress for each of the experimental runs is the same. It can be seen that the spatial pattern of $\bar{u}/\langle\bar{u}\rangle$ still changes with relative submergence, but that the changes are more subtle. There is again evidence of an alternating pattern of streamwise streaks of high- and low-speed fluid, and also, similar low-speed spots appear on these streaks. An increase in relative submergence causes the number of high-speed streaks over the bed to decrease and the low-speed spots to become larger. A number of spots which appear at the lower submergences do not appear at the higher submergences. The overall cause is that at the highest relative submergence, the measurement area is only dominated by one large high-speed streak.

Similar broad changes in the spatial pattern with relative submergence can also be seen in Figure 6 for the bimodal bed. Again the changes are less apparent than was seen at a single bed slope. In summary, there appears to a common pattern over both beds, with very weak spatial patterns in $\bar{u}/\langle\bar{u}\rangle$ at very low submergences, and as submergence increases, strong streamwise organisation is seen. This organisation then weakens again and eventually disappears about a higher level of submergence.

Correlation between the Spatial Organisation of Time-averaged Streamwise Velocity and Bed Surface Topography

The Digital Elevation Model (DEM) for the unimodal bed is shown in Figure 7a. If there was a simple correlation between bed surface elevation z_b and $\bar{u}/\langle\bar{u}\rangle$, this topography would suggest that there would be matching areas of higher and lower velocity caused by the bed surface. It is evident that in no contour plots of $\bar{u}/\langle\bar{u}\rangle$ does this occur. Many of the plots instead display a greater number of high-speed streaks (and in some cases low-speed streaks) than such a correlation would indicate. It would appear that the large-scale organisation of $\bar{u}/\langle\bar{u}\rangle$ over the bed does not resemble that of the bed surface elevations. This is also seen over the bimodal bed (Figure 7b). The fact that high-speed streaks were found to occur over both beds, which have different surface topographies, further indicates that bed surface topography may not have induced such features.

There were small, discrete areas of the bed experiencing slower than average flow over both beds. These varied in size from approximately D_{50} around two to four D_{50}. There are localised areas of higher and lower elevations over both beds that could induce flow features like these. It could be that the small-scale organisation of $\bar{u}/\langle\bar{u}\rangle$ may be better associated with the surface topography of the bed. However, a visual comparison between the DEM of the two beds and the spatial pattern of $\bar{u}/\langle\bar{u}\rangle$ suggests that this is unlikely.

However, to discover whether there is any association between the spatial pattern of $\bar{u}/\langle\bar{u}\rangle$ and the bed surface topography a more formal examination is required. This is achieved through a simple cross-correlation between $\bar{u}/\langle\bar{u}\rangle$ and z_b based on the approach used by Legleiter *et al.* (2007). A cross-correlogram was used to quantify the spatial covariance between pairs of $\bar{u}/\langle\bar{u}\rangle$ and z_b measurements. A series of streamwise lags l_x and lateral

lags l_y between $\bar{u}/\langle\bar{u}\rangle$ and z_b were applied to take into account, respectively, the streamwise and lateral propagation of the flow relative to the bed. Using a cross-correlogram in this way means that the cross-covariance C between $\bar{u}/\langle\bar{u}\rangle$ and z_b is given by

$$C(l_{i,j}) = \frac{1}{N(l_{i,j})} \sum_{x=3.15}^{N(l_{i,j})} \frac{\bar{u}}{\langle\bar{u}\rangle}(x_{i,j}) \cdot z_b(x_{i,j} + l_{i,j}) - m_{i,j} \cdot n_{i,j} \tag{1}$$

where

$$m_{i,j} = \frac{1}{N(l_{i,j})} \sum_{x=3.15}^{N(l_{i,j})} \frac{\bar{u}}{\langle\bar{u}\rangle}(x_{i,j}) \tag{2}$$

and

$$n_{i,j} = \frac{1}{N(l_{i,j})} \sum_{x=3.15}^{N(l_{i,j})} z_b(x_{i,j} + l_{i,j}) \tag{3}$$

and N is the number of cross-correlated measurements and $x_{i,j}$ is the co-ordinate position within the measurement area. The C values depend on the magnitudes of $\bar{u}/\langle\bar{u}\rangle$ and z_b so a cross-correlogram was used to calculate the correlation coefficient η to provide a more bounded measure of spatial cross-correlation (Legleiter *et al.*, 2007):

$$\eta(l_{i,j}) = \frac{C(l_{i,j})}{\sqrt{\sigma_{fi,j}^2 \cdot \sigma_{bi,j}^2}} \in [-1,+1] \tag{4}$$

where

$$\sigma_{fi,j}^2 = \frac{1}{N(l_{i,j})} \sum_{x=3.15}^{N(l_{i,j})} \left[\frac{\bar{u}}{\langle\bar{u}\rangle}(x_{i,j}) - m_{i,j} \right]^2 \tag{5}$$

and

$$\sigma_{bi,j}^2 = \frac{1}{N(l_{i,j})} \sum_{x=3.15}^{N(l_{i,j})} \left[z_b(x_{i,j} - l_{i,j}) - n_{i,j} \right]^2 \tag{6}$$

In this way, it provides a measure of the strength of the linear association between $\bar{u}/\langle\bar{u}\rangle$ and z_b at the grain-scale. A minimum value of -100 mm was chosen for l_x to account fully for the propagation of the flow possible for the range of $\langle\bar{u}\rangle$ values. A cross-correlation between $\bar{u}/\langle\bar{u}\rangle$ and z_b was also applied for $-25 \leq l_y \leq 25$ mm, allowing for a lateral movement of the flow relative to the bed of a range of $10D_{50}$ and $11D_{50}$ for the unimodal and bimodal beds, respectively.

The cross-correlation was first performed using the streamwise and lateral lags for all the available $\bar{u}/\langle\bar{u}\rangle$ values. Then two additional cross-correlation analyses were undertaken using restricted values of $\bar{u}/\langle\bar{u}\rangle$, where $\bar{u}/\langle\bar{u}\rangle > 1$ and where $\bar{u}/\langle\bar{u}\rangle < 0.9$. This was to examine whether there is a lesser or greater correlation between the high-speed and low-speed flow features with the bed surface topography, respectively. Therefore the latter two correlations should provide information on whether the large-scale and/or the small-scale organisation of the flow is related to the bed surface topography.

The η values are shown in Figure 8 for the experimental runs performed at a single bed slope over the unimodal bed when a streamwise lag is applied. A η value of 1 indicates that there is a perfect linear positive correlation between $\bar{u}/\langle\bar{u}\rangle$ and z_b, -1 that there is a perfect linear negative correlation, and 0 that there is almost no linear correlation. The results show that for the correlation involving all the $\bar{u}/\langle\bar{u}\rangle$ values, there is a poor linear association between $\bar{u}/\langle\bar{u}\rangle$ and z_b. There is a tendency for the correlation to improve with an increase in relative submergence. The correlation is also poor for values of $\bar{u}/\langle\bar{u}\rangle > 1$. This also applies for $\bar{u}/\langle\bar{u}\rangle < 0.9$, expect for the experimental run performed at the lowest relative submergence of 1.2. There is also a tendency for the correlation to improve with a decrease in relative submergence. When a lateral lag is applied between $\bar{u}/\langle\bar{u}\rangle$ and z_b, very similar results are shown (Figure 9). The association between $\bar{u}/\langle\bar{u}\rangle$ and z_b again displays a tendency to improve with relative submergence when the correlation involves all the $\bar{u}/\langle\bar{u}\rangle$ values, and to do the reverse for $\bar{u}/\langle\bar{u}\rangle < 0.9$. Once again only the run at a relative submergence of 1.2 shows any reasonable correlation when both all the $\bar{u}/\langle\bar{u}\rangle$ values are used and when $\bar{u}/\langle\bar{u}\rangle < 0.9$.

Over the bimodal bed for the experimental runs performed at a single bed slope, the relationship between $\bar{u}/\langle\bar{u}\rangle$ and z_b is even poorer (Figures 10 and 11). There is a noticeable decrease in the difference in η between the experimental runs, and relative submergence does not appear to influence η, which was not seen over the unimodal bed. Very similar results were also found for the experimental runs performed at the same mean bed shear stress over both beds, which is expected given that the spatial pattern of $\bar{u}/\langle\bar{u}\rangle$ for these runs was similar to that at a single bed slope.

The results clearly show that neither the large-scale or small-scale spatial organisation of $\bar{u}/\langle\bar{u}\rangle$ is related in any simple linear manner to the bed surface elevation over either of the beds. However, given that a η value of zero does not necessarily mean that there is no correlation at all, the results do not rule out any subtle or more complicated association between $\bar{u}/\langle\bar{u}\rangle$ and z_b, such as a high non-linear correlation, or a relationship between $\bar{u}/\langle\bar{u}\rangle$ and any spatially coherent or large-scale bed features. The results of the cross-correlation are not surprising given the DEMs (Figure 7) indicated that the beds were organised in a different manner, yet there is a remarkable similarity in the spatial pattern of $\bar{u}/\langle\bar{u}\rangle$. Relative submergence does not consistently influence the strength of the association between $\bar{u}/\langle\bar{u}\rangle$ and z_b over the two beds, which opposes the conclusion of Legleiter *et al.* (2007). This is likely to be because, unlike the bed studied by Legleiter *et*

al., there are no large roughness elements on the surface in which their effects would become drowned out with an increase in relative submergence.

4. DISCUSSION

The existence of streamwise streaks of high-speed fluid which decrease in number with an increase in relative submergence could be said to reflect the presence of secondary currents within the flume. Detailed measurements were made within the flume to determine whether secondary currents exist. Nine PIV measurements in a vertical plane were taken across the flume at equal intervals, which provided measurements of streamwise and vertical velocities. If secondary cells exist within the flow, then the expectation would be that the double-averaged vertical velocity on the centreline of the flume would be non-zero. This would be because the cells are symmetrical on either lateral side of the centreline. But analysis of the vertical plane PIV measurements for all experimental runs revealed that this is not the case. The occurrence of two-dimensional flow within the measurement section was further assured by ensuring that the measurement section was a sufficient distance from the inlet and weir of the flume, and from the upstream and downstream fixed bed sections, given the depth of the flows (Kırkgöz and Ardıçlıoğlu, 1997). A number of studies have examined the conditions within which the flow can be considered two-dimensional in terms of the ratio of flume width to flow depth w/d. These conditions have been said to occur if $w/d > 3.5$ (Song *et al.*, 1994) or if $w/d > 5$ (Nezu and Nakagawa, 1993; Kironoto and Graf, 1994). All the experimental runs satisfied these conditions.

It is interesting to note that the streaky spatial pattern described in this paper does display some parallels to the spatial structure that has been observed for turbulent, instantaneous flow fields. Kline *et al.* (1967) was one of the first to discover this pattern. Using hydrogen bubble visualisation they observed that the flow was organised into long, spatially separated streaks which were essentially aligned in the streamwise direction. It resulted in a lateral alternating pattern of regions of relatively high-speed and low-speed regions. The instantaneous streamwise velocities within this latter region were retarded relative to the time-averaged velocity and have been termed low-speed streaks. In the regions between the steaks, the instantaneous streamwise velocities were in excess of the time-averaged velocity and were therefore termed high-speed regions or streaks. They are known to be a persistent and dominant feature of the near-wall flow for both smooth and rough boundaries (Smith and Metzler, 1983; Smith *et al.*, 1991; Grass *et al.*, 1991; Nezu and Nakagawa, 1993; Defina, 1996; Grass and Mansour-Tehrani, 1996). It has been evident, for example, over regularly packed spheres and gravel clasts. This streaky pattern has also been shown to occur for atmospheric boundary layers (e.g. Klewicki *et al.*, 1995; Schoppa and Hussain, 2002; Drobinski and Foster, 2003; Kanda *et al.*, 2004). Further information on low-speed streaks and the mechanism of their formation can be found in a review by Smith (1996).

A further similarity between patterns observed in $\bar{u}/\langle\bar{u}\rangle$ and this instantaneous streaky pattern is the way in which the pattern changes with height above the boundary. Measurements of the instantaneous velocity flow field and further streamwise observations of this pattern (e.g. Smith and Schwartz, 1983) have shown that it persists at a good distance from the boundary. This was also seen for $\bar{u}/\langle\bar{u}\rangle$ in Cooper (2006). Furthermore, the instantaneous streaky pattern has been shown to become progressively more broadly

spaced, and less organised, until it essentially disappears (Smith, 1996). Again this was observed for $\bar{u}/\langle\bar{u}\rangle$ (Cooper, 2006).

The fact that the instantaneous streaky pattern has been found over boundaries of various roughness and bed configurations has led many to believe that these streaks are a universal feature of boundary layer turbulence irrespective of wall roughness condition (Grass and Mansour-Tehrani, 1996, Smith, 1996). Grass *et al.* (1991) said that the remarkable feature of rough wall flow is the apparent ability to order itself very rapidly over a small vertical distance above the roughness elements and for it to be decoupled from the local influence of individual elements. The bed surface topographies of the unimodal and bimodal bed were different and yet produced a similar pattern of $\bar{u}/\langle\bar{u}\rangle$ over the bed, and showed no strong linear correlation with bed surface elevation, which is in line with these thoughts.

The similarity between the spatial patterns of $\bar{u}/\langle\bar{u}\rangle$ and the instantaneous flow field does not necessarily suggest that what has been observed in the spatial pattern of $\bar{u}/\langle\bar{u}\rangle$ is a result of these turbulent features. To determine this, an analysis of the frequency of occurrence of this pattern within the instantaneous flow fields and the magnitude of the turbulent features (in terms of the departure of instantaneous streamwise velocity from $\bar{u}$ at each spatial location) would have to be performed. For the instantaneous streaky pattern to be observed within the time-averaged flow field it would mean that it must be both temporally and spatially persistent. In other words it must occur in the same location, be large enough in magnitude and occur frequently enough to still appear after time averaging. Previous studies do not provide any extensive information on whether this would be possible. But interestingly, Grass and Mansour-Tehrani (1996) found over a gravel boundary that low-speed streaks randomly shift their lateral position with time.

Spatially coherent time-averaged flow structures have also been observed over smooth boundaries. Large, outer region structures which appear to span the majority of the turbulent boundary layer and dominate the flow when viewed on a time-averaged basis have been reported (e.g. Kovasznay *et al.*, 1970; Falco, 1977; Smith *et al.*, 1991). However, while significant energy is contained within these motions, Smith (1996) believes that they are inactive, dissipative and extract little energy from the time-averaged flow. Time-averaged vortical structures between regularly spaced 2-D transverse ribs (Pokrajac *et al.*, 2007) and over fixed 2-D dune shaped bedforms (Coleman *et al.*, 2006) have also been discovered. Numerical simulations of airflow over arrays of cubes to simulate urban-like roughness using Large Eddy Simulation (Kanda *et al.*, 2004), Reynolds-averaged Navier-Stokes equations (Lien and Yee, 2004) and double-averaged Navier-Stokes equations (Coceal *et al.*, 2006) have also discovered the same structures.

In regard to the small, discrete areas of the bed experiencing slower than average flow over both of the beds, they are unlikely to be just transient eddies because of the length of the time-averaging window. It implies that the fixed-location spots may be caused by repeated bursting from certain locations on the bed.

The general changes that have been observed in the spatial organisation of $\bar{u}/\langle\bar{u}\rangle$ with relative submergence also resemble those discovered by Legleiter *et al.* (2007). They concluded that an increase in flow stage results in the spatial structure of $\bar{u}$ becoming smoother and more continuous. This is consistent with our observations that increases in relative submergence cause an overall increase in the homogeneity of the distribution of $\bar{u}$

over the bed. The observation that the spatial organisation of $\bar{u}$ is not strongly related in a simple manner with grain-scale bed surface topography also supports the findings of Lamarre and Roy (2005) and Legleiter *et al.* (2007) at the reach-scale. Both of these studies also describe similar conclusions over the relative influence of relative submergence and bed surface topography on the spatial distribution of $\bar{u}$. Lamarre and Roy (2005) found that, in a gravel-bed river, roughness elements had surprisingly little impact on the flow at the reach-scale, despite a topographically complex channel boundary. Boulders and pebble clusters were found to only affect the flow over a relatively small proportion of the reach. The complexity of the bed surface topography on the bed was not reflected in the spatial variability of vertical profiles of $\bar{u}$. The large majority of profiles were logarithmic (75%), leading to the suggestion that the similarity in the shape of the profiles might be the result of bed stability created by the spatial organisation of bed surface features at low submergences. As a result, they concluded that the distribution of the mean flow properties displayed a well organised, coherent spatial pattern that was controlled by flow depth rather than by abrupt, isolated changes associated with individual clasts. Legleiter *et al.* (2007) also discovered results which supported these claims, even in flows where the flow depth was of the same order as the D_{84} of the bed. Individual roughness elements were found to have little linear correlation with the flow, and that flow depth had a fundamental control on flow structure through its influence on the spatial persistence of the flow.

Similar conclusions can also be drawn from the results presented in this paper. It is striking that despite the clear differences in the bed surface topography of the two beds they both display a similar spatial organisation of $\bar{u}/\langle\bar{u}\rangle$. A change in relative submergence was also shown to result in the same broad changes in the spatial pattern on $\bar{u}/\langle\bar{u}\rangle$ over the two beds. On average, an increase in relative submergence caused a decrease in the number of high-speed streaks, and an enlarging of the low-speed spots. Therefore, overall it caused an increase in the homogeneity of the distribution of time-averaged streamwise velocities over the bed. This was the case both at a single bed slope and for those runs performed at the same mean bed shear stress, demonstrating that relative submergence had a consistent influence on the spatial pattern of $\bar{u}/\langle\bar{u}\rangle$. Since these changes in the spatial pattern of $\bar{u}/\langle\bar{u}\rangle$ with relative submergence were observed from measurements at the same z/k, it demonstrated that the effect of the roughness of the bed cannot fully account for the variability in the spatial pattern between the experimental runs. It is therefore suggested that bed surface topography at the grain-scale exerted less of an influence on the spatial organisation of $\bar{u}/\langle\bar{u}\rangle$ than relative submergence. Although no examination was made of the spatial structure of turbulent flow structures, it is interesting that this supports the conclusion of Roy *et al.* (2004) that flow depth is the fundamental control on flow structure.

5. CONCLUSIONS

The spatial organisation of time-averaged streamwise velocities in the near-bed region over two water-worked gravel beds has been characterised in detail. It has been examined how this organisation changes with relative submergence and whether it is correlated with bed surface topography at the grain-scale. It was discovered that there is considerable spatial variability in time-averaged streamwise velocities over the two beds. Particular areas of the bed experienced values as low as 70 % of the double-averaged streamwise velocity. The velocities displayed a considerable degree of organisation in the near-bed region. They

were organised into streamwise streaks of high-speed fluid which were overlain by spots of low-speed fluid. This pattern was consistent over the two beds and indicated the presence of spatially coherent time-averaged flow structures. This spatial pattern was found to be consistently and heavily dependent on relative submergence, both for tests carried out at a single bed slope and those performed at the same mean bed shear stress. Increases in relative submergence were shown to cause a progressive decrease in the number of high-speed streaks over the bed, and their eventual disappearance. This was accompanied by a reduction in the distinction and spatial persistence of the low-speed spots, and an overall increase in the homogeneity of the distribution of time-averaged streamwise velocities over the bed.

A key discovery was that the spatial pattern of time-averaged streamwise velocities had little linear coherence with bed surface topography. It was shown that neither the large-scale or small-scale flow organisation was well associated with the bed surface elevations of either of the beds. Given that the changes in spatial organisation were related to changes in relative submergence, it suggested that for flows above the bed, bed surface topography at the grain-scale exerted less of an influence on the spatial organisation of time-averaged streamwise velocities than relative submergence.

Acknowledgements

References

Barison, S., A. Chegini, A. Marion, and S.J. Tait, 2003, *Modifications in near bed flow over sediment beds and the implications for grain entrainment*, Proceedings of XXX IAHR Congress, Thessalonki, Greece, 509-516.

Buffin-Bélanger, T., and A.G. Roy, 1998, *Effects of a pebble cluster on the turbulent structure of a depth-limited flow in a gravel-bed river*, Geomorphology **25**, 3-4, 249-267.

Campbell, L., I. McEwan, V. Nikora, D. Pokrajac, M. Gallagher, and C. Manes, 2005, *Bed-load effects on hydrodynamics of rough-bed open-channel flows*, Journal of Hydraulic Engineering, ASCE **131**, 7, 576-585.

Carling, P.A., Z.X. Cao, M.J. Holland, D.A. Ervine, and K. Babaeyan-Koopaei, 2002, *Turbulent flow across a natural compound channel*, Water Resources Research **38**, 12, 6-11.

Clifford, N.J., 1996, *Morphology and stage-dependent flow structure in a gravel-bed river*. In Ashworth, P.J., Bennett, S.J., Best, J.L., McLelland, S.J. (eds), Coherent Flow Structures in Open Channels, John Wiley & Sons, Chichester, 545-566.

Coceal, O., T.G. Thomas, I.P. Castro, and S.E. Belcher, 2006, *Mean flow and turbulence statistics over groups of urban-like cubical obstacles*, Boundary-Layer Meteorology **121**, 491-519.

Coleman, S.E., V.I. Nikora, S.R. McLean, T.M. Clunie, T. Schlicke, and B.W. Melville, 2006, *Equilibrium hydrodynamics concept for developing dunes*, Physics of Fluids **18**, 10, doi: 10.1063/1061.2358332.

Cooper, J.R., 2006, *Spatially-induced momentum transfer over water-worked gravel beds*, PhD Thesis, University of Sheffield, Sheffield, UK.

Dantec, 2000, *FlowMap Particle Image Velocimetry Instrumentation: Installation and Users Guide*, Dantec Measurement Technology, Skovlunde.

Defina, A., 1996, *Transverse spacing of low-speed streaks in a channel flow over a rough bed*. In Ashworth, P.J., Bennett, S.J., Best, J.L., McLelland, S.J. (eds), Coherent Flow Structures in Open Channels, John Wiley & Sons, Chichester, 87-99.

Drobinski, P., and R.C. Foster, 2003, *On the origin of near-surface streaks in the neutrally-stratified planetary boundary layer*, Boundary-Layer Meteorology **108**, 2, 247-256.

Falco, R.E., 1977, *Coherent motions in outer region of turbulent boundary-layers*, Physics of Fluids **20**, 10, S124-S132.

Grass, A.J., and M. Mansour-Tehrani, 1996, *Generalized scaling of coherent bursting structures in the near-wall region of turbulent flow over smooth and rough boundaries*. In Ashworth, P.J., Bennett, S.J., Best, J.L., McLelland, S.J. (eds), Coherent Flow Structures in Open Channels, John Wiley & Sons, Chichester, 40-61.

Grass, A.J., R.J. Stuart, and M. Mansour-Tehrani, 1991, *Vortical structures and coherent motion in turbulent-flow over smooth and rough boundaries*, Philosophical Transactions of the Royal Society of London Series A - Mathematical Physical and Engineering Sciences **336**, 1640, 35-65.

Kanda, M., R. Moriwaki, and F. Kasamatsu, 2004, *Large-eddy simulation of turbulent organized structures within and above explicitly resolved cube arrays*, Boundary-Layer Meteorology **112**, 2, 343-368.

Kırkgöz M.S. and M. Ardıçlıoğlu, 1997, *Velocity profiles of developing and developed open channel flow*, Journal of Hydraulic Engineering, ASCE **123**, 12, 1099-1105.

Kironoto, B.A., and W.H. Graf, 1994, *Turbulence characteristics in rough uniform open-channel flow*, Proceedings of the Institution of Civil Engineers - Water Maritime and Energy **106**, 4, 333-344.

Klewicki, J.C., M.M. Metzger, E. Kelner, and E.M. Thurlow, 1995, *Viscous sublayer flow visualizations at $R_\theta \approx 1\,500\,000$*, Physics of Fluids **7**, 4, 857-863.

Kline, S.J., W.C. Reynolds, F.A. Schraub, and P.W. Runstadler, 1967, *The structure of turbulent boundary layers*, Journal of Fluid Mechanics **30**, 741-773.

Kovasznay, L.S., V. Kibens, and R.F. Blackwelder, 1970, *Large-scale motion in intermittent region of a turbulent boundary layer*, Journal of Fluid Mechanics **41**, 283-325.

Lamarre, H., and A.G. Roy, 2005, *Reach scale variability of turbulent flow characteristics in a gravel-bed river*, Geomorphology **68**, 1-2, 95-113.

Lane, S.N., R.J. Hardy, L. Elliott, and D.B. Ingham, 2002, *High-resolution numerical modelling of three-dimensional flows over complex river bed topography*, Hydrological Processes **16**, 11, 2261-2272.

Lane, S.N., R.J. Hardy, L. Elliott, and D.B. Ingham, 2004, *Numerical modeling of flow processes over gravelly surfaces using structured grids and a numerical porosity treatment*, Water Resources Research **40**, 1, doi: 40:W01302JAN82004.

Lawless, M., and A. Robert, 2001, *Scales of boundary resistance in coarse-grained channels: turbulent velocity profiles and implications*, Geomorphology **39**, 3-4, 221-238.

Legleiter, C.J., T.L. Phelps, and E.E. Wohl, 2007, *Geostatistical analysis of the effects of stage and roughness on reach-scale spatial patterns of velocity and turbulence intensity*, Geomorphology **83**, 322-345.

Lien, F.S., and E. Yee, 2004, *Numerical modelling of the turbulent flow developing within and over a 3-D building array, part I: a high-resolution Reynolds-averaged Navier-Stokes approach*, Boundary-Layer Meteorology **112**, 3, 427-466.

McLelland, S.J., P.J. Ashworth, J.L. Best, and J.R. Livesey, 1999, *Turbulence and secondary flow over sediment stripes in weakly bimodal bed material*, Journal of Hydraulic Engineering, ASCE **125**, 5, 463-473.

Nezu, I., and H. Nakagawa, 1993, *Turbulence in open channel flows*, A. A. Balkema, Rotterdam.

Nikora, V., D. Goring, I. McEwan, and G. Griffiths, 2001, *Spatially averaged open-channel flow over rough bed*, Journal of Hydraulic Engineering, ASCE **127**, 2, 123-133.

Paola, C., G. Parker, R. Seal, S.K. Sinha, J.B. Southard, and P.R. Wilcock, 1992, *Downstream fining by selective deposition in a laboratory flume*, Science **258**, 1757-1760.

Papanicolaou, A.N., and R. Hilldale, 2002, *Turbulence characteristics in gradual channel transition*, Journal of Engineering Mechanics, ASCE **128**, 9, 948-960.

Pokrajac, D., L.J. Campbell, V. Nikora, C. Manes, and I. McEwan, 2007, *Quadrant analysis of persistent spatial velocity perturbations over square-bar roughness*, Experiments in Fluids **42**, 3, 413-423.

Roy, A.G., T. Buffin-Belanger, H. Lamarre, and A.D. Kirkbride, 2004, *Size, shape and dynamics of large-scale turbulent flow structures in a gravel-bed river*, Journal of Fluid Mechanics **500**, 1-27.

Sambrook Smith, G.H.S., and A.P. Nicholas, 2005, *Effect on flow structure of sand deposition on a gravel bed: results from a two-dimensional flume experiment*, Water Resources Research **41**, 10, doi: 10:1029/2004WR003817.

Schoppa, W., and F. Hussain, 2002, *Coherent structure generation in near-wall turbulence*, Journal of Fluid Mechanics **453**, 57-108.

Seal, R., C. Paola, G. Parker, J.B. Southard, and P.R. Wilcock, 1997, *Experiments on downstream fining of gravel: 1. narrow-channel runs*, Journal of Hydraulic Engineering, ASCE **123**, 10, 874-884.

Smith, C.R., 1996, *Coherent flow structures in smooth-wall turbulent boundary layers: facts, mechanisms and speculation*. In Ashworth, P.J., Bennett, S.J., Best, J.L., McLelland, S.J. (eds), Coherent Flow Structures in Open Channels, John Wiley & Sons, Chichester, 1-39.

Smith, C.R., and S.P. Metzler, 1983, *The characteristics of low-speed streaks in the near-wall region of a turbulent boundary-layer*, Journal of Fluid Mechanics **129**, 27-54.

Smith, C.R., and S.P. Schwartz, 1983, *Observation of streamwise rotation in the near-wall region of a turbulent boundary-layer*, Physics of Fluids **26**, 3, 641-652.

Smith, C.R., J.D.A. Walker, A.H. Haidari, and U. Soburn, 1991, *On the dynamics of near-wall turbulence*, Philosophical Transactions of the Royal Society of London, Series A **336**, 131-175.

Song, T., U. Lemmin, and W.H. Graf, 1994, *Uniform-Flow in Open Channels with Movable Gravel-Bed*, Journal of Hydraulic Research **32**, 6, 861-876.

Tait, S.J., B.B. Willetts, and M.W. Gallagher, 1996, *The application of Particle Image Velocimetry to the study of coherent flow structures over a stabilizing sediment bed*. In Ashworth, P.J., Bennett, S.J., Best, J.L., McLelland, S.J. (eds), Coherent Flow Structures in Open Channels, John Wiley & Sons, Chichester, 184-201.

Toro-Escobar, C.M., C. Paola, G. Parker, P.R. Wilcock, and J.B. Southard, 2000, *Experiments on downstream fining of gravel: II. wide and sandy runs*, Journal of Hydraulic Engineering, ASCE **126**, 3, 198-208.

Tritico, H.M., and R.H. Hotchkiss, 2005, *Unobstructed and obstructed turbulent flow in gravel bed rivers*, Journal of Hydraulic Engineering, ASCE **131**, 8, 635-645.

Westerweel, J., 1994, *Efficient detection of spurious vectors in Particle Image Velocimetry data*, Experiments in Fluids **16**, 3-4, 236-247.

Table 1. A summary of the experimental conditions over the unimodal bed, where S is the bed slope, Q is the flow discharge, d is the flow depth, k is the thickness of the interfacial sublayer, w is the width of the flume, $\overline{U}$ is the average flow velocity (calculated from the ratio of Q to the cross-sectional area of the flow), τ_0 is the bed shear stress (calculated from the depth-slope product), Re is the flow Reynolds number and Fr is the Froude number.

Run	S	Q (m³/s)	d (m)	d/k	w/d	$\overline{U}$ (m/s)	τ_0 (N/m²)	Re	Fr
1	0.00285	0.00159	0.0181	1.2	27.6	0.18	0.47	2427	0.42
2	0.00285	0.00389	0.0286	1.9	17.5	0.27	0.72	5933	0.51
3	0.00285	0.00635	0.0395	2.6	12.7	0.32	0.95	9680	0.52
4	0.00285	0.00869	0.0484	3.2	10.3	0.36	1.13	13246	0.52
5	0.00285	0.0140	0.0628	4.1	8.0	0.45	1.40	21339	0.57
6	0.00285	0.0280	0.0900	5.9	5.6	0.62	1.85	42618	0.66
7	0.00375	0.0162	0.0635	4.2	7.9	0.51	1.86	24750	0.65
8	0.00465	0.0123	0.0492	3.2	10.2	0.50	1.87	18720	0.72
9	0.00555	0.00978	0.0399	2.6	12.5	0.49	1.87	14905	0.78
10	0.00645	0.00692	0.0335	2.2	14.9	0.41	1.87	10546	0.72
11	0.00735	0.00655	0.0295	1.9	16.9	0.44	1.90	9977	0.83

Table 2. A summary of the experimental conditions over the biimodal bed, where S is the bed slope, Q is the flow discharge, d is the flow depth, k is the thickness of the interfacial sublayer, w is the width of the flume, $\overline{U}$ is the average flow velocity (calculated from the ratio of Q to the cross-sectional area of the flow), τ_0 is the bed shear stress (calculated from the depth-slope product), Re is the flow Reynolds number and Fr is the Froude number.

Run	S	Q (m³/s)	d (m)	d/k	w/d	$\overline{U}$ (m/s)	τ_0 (N/m²)	Re	Fr
12	0.00284	0.00143	0.0173	1.3	28.9	0.16	0.45	2171	0.40
13	0.00284	0.00276	0.0272	2.0	18.4	0.20	0.68	4198	0.39
14	0.00284	0.00527	0.0373	2.7	13.4	0.28	0.90	8029	0.47
15	0.00284	0.00809	0.0455	3.3	11.0	0.36	1.07	12333	0.53
16	0.00284	0.0127	0.0595	4.3	8.4	0.43	1.34	19333	0.56
17	0.00284	0.0245	0.0845	6.2	5.9	0.58	1.76	37388	0.64
18	0.00374	0.01400	0.0594	4.3	8.4	0.47	1.76	21339	0.62
19	0.00464	0.0111	0.0472	3.4	10.6	0.47	1.80	16921	0.69
20	0.00554	0.00728	0.0371	2.7	13.5	0.39	1.75	11087	0.65
21	0.00644	0.00550	0.0317	2.3	15.8	0.35	1.77	8385	0.62
22	0.00734	0.00356	0.0268	2.0	18.7	0.27	1.74	5417	0.52
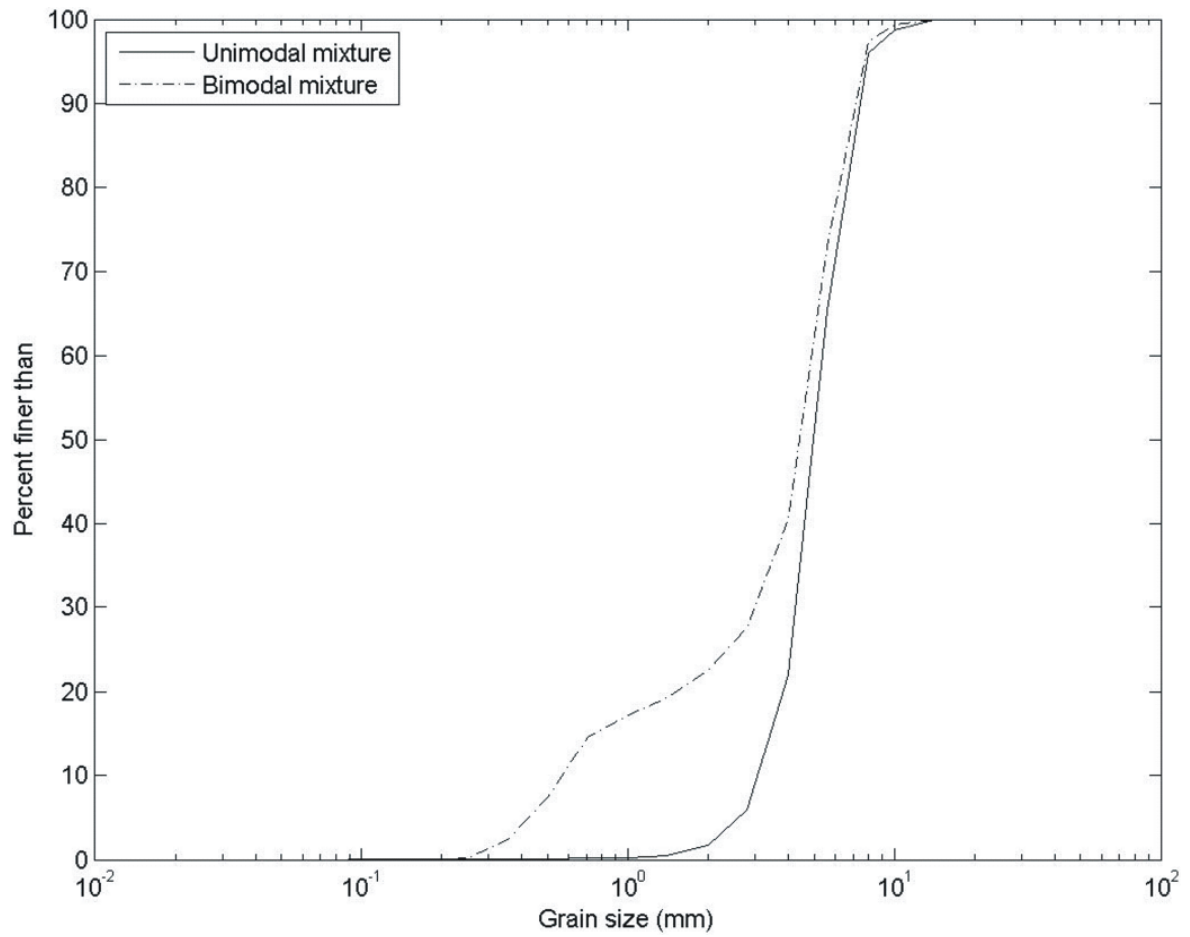
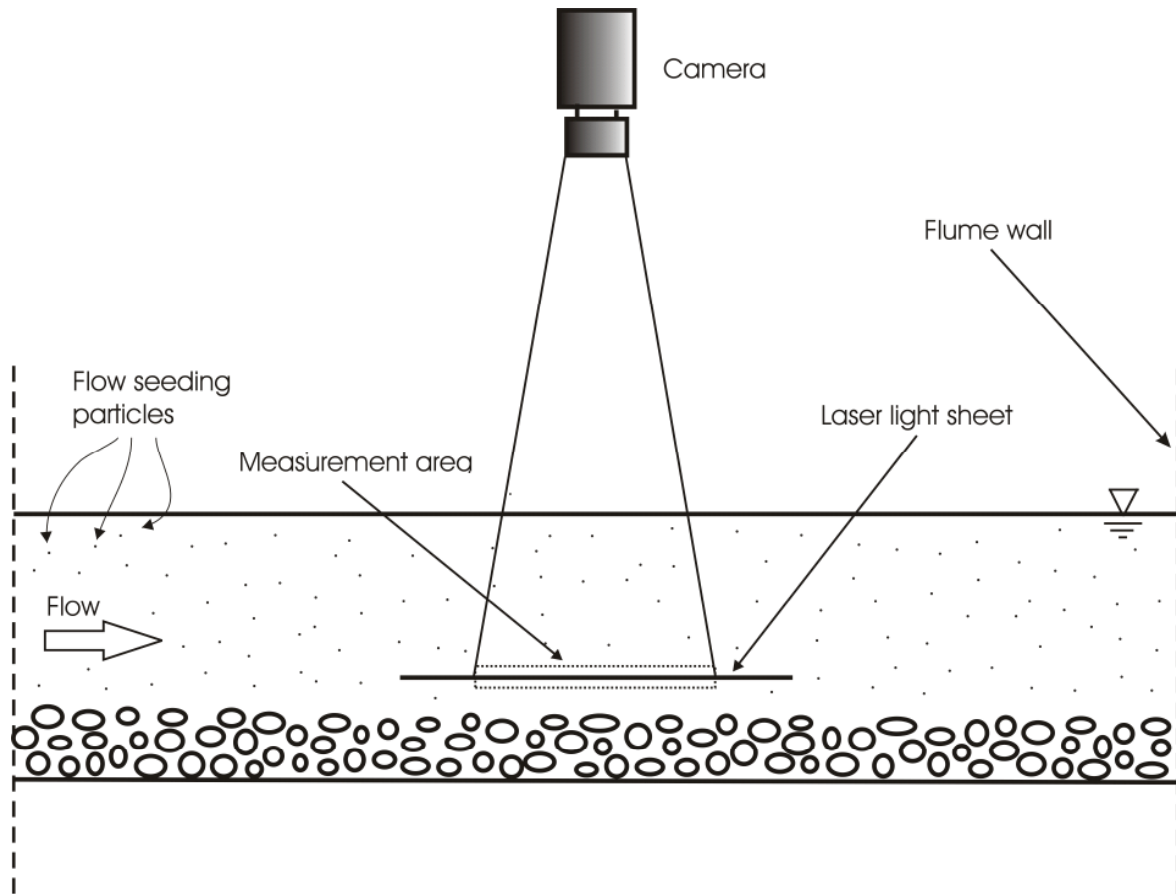**Figure 1.** Grain-size distributions of the two mixtures used to form the two beds.

Figure 2. A schematic of the Particle Image Velocimetry configuration.
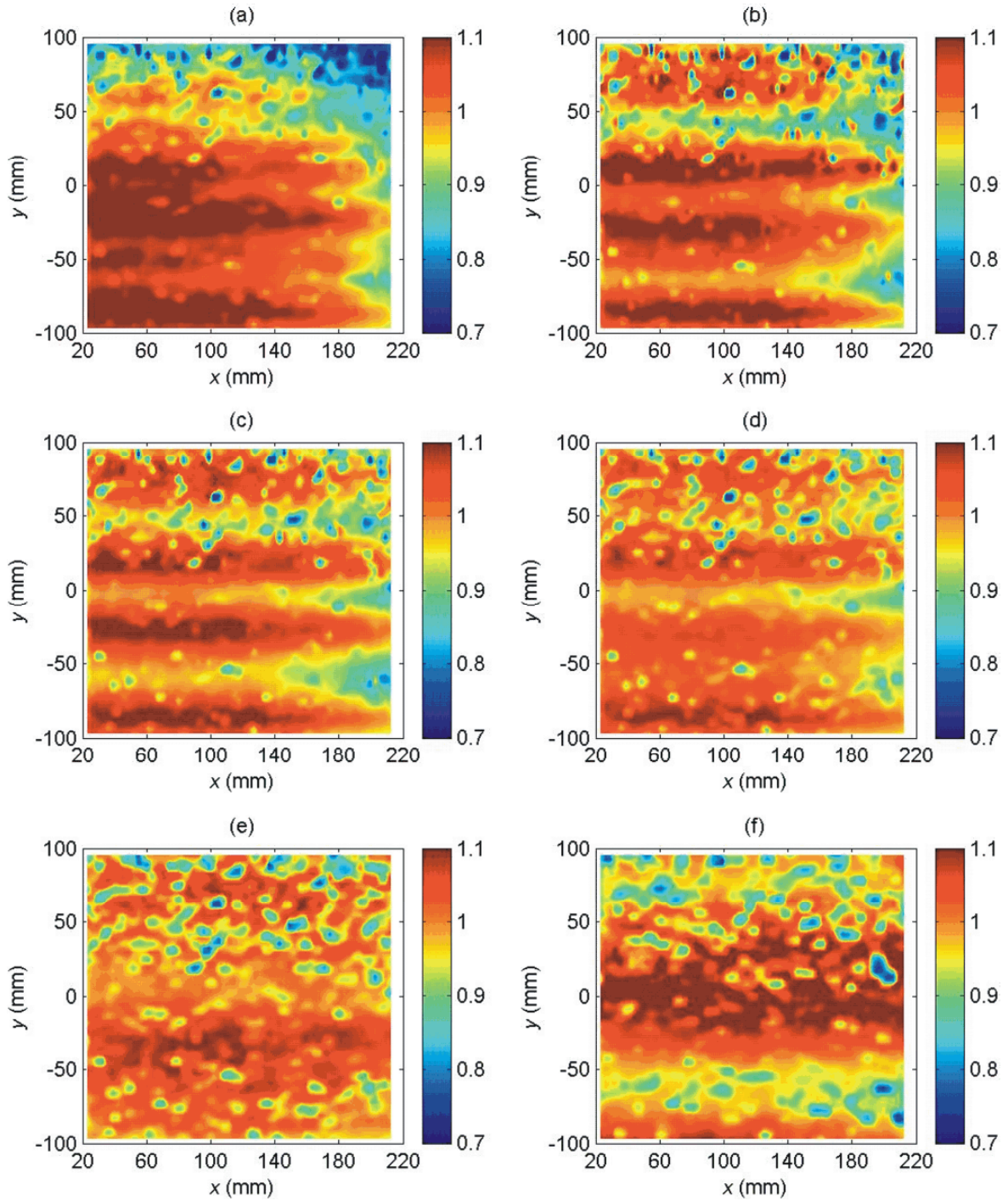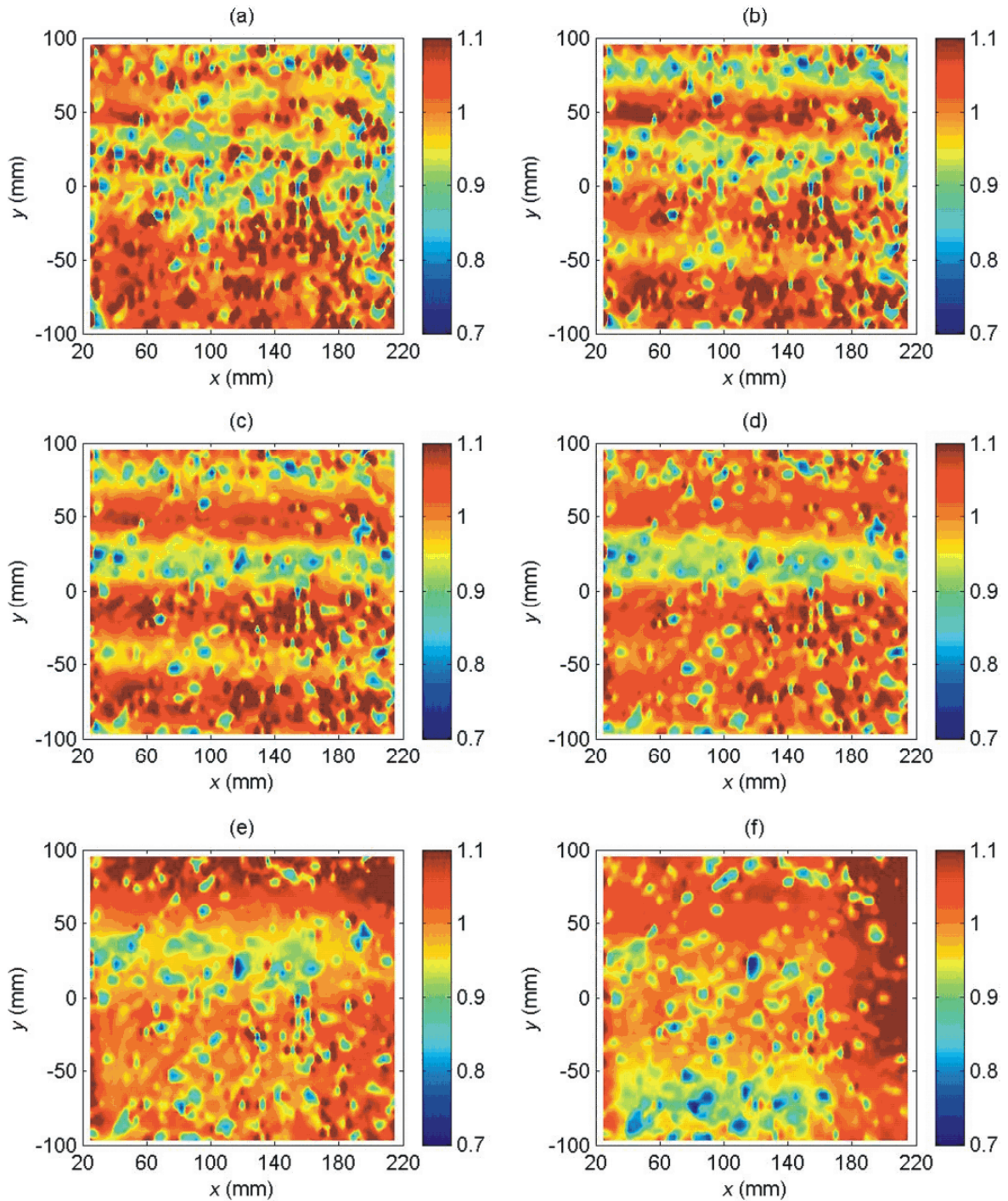
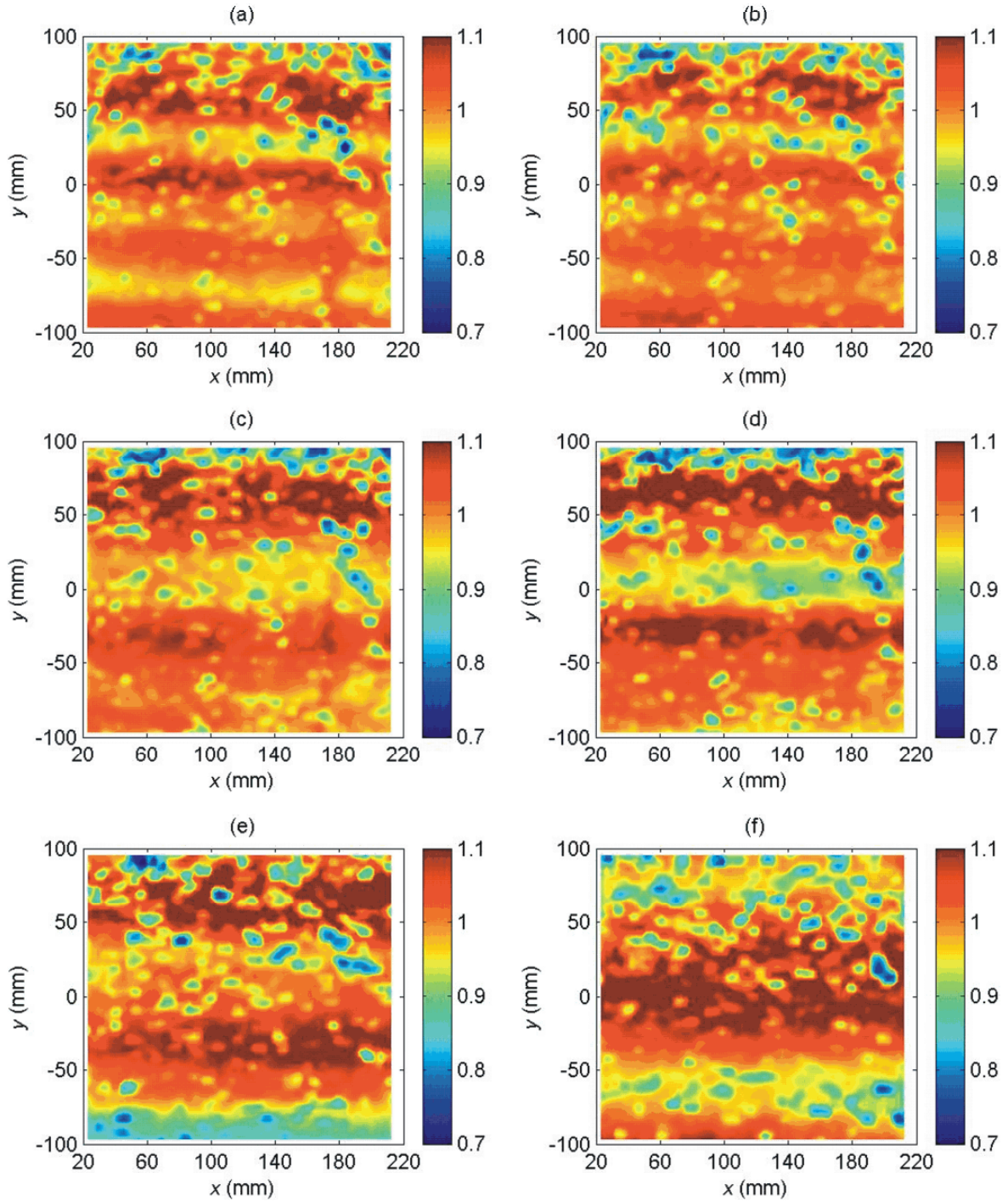**Figure 3.** The spatial distribution of $\bar{u}/\langle\bar{u}\rangle$ over the unimodal bed for the experimental runs performed at a single bed slope with (a) $d/k = 1.2$; (b) $d/k = 1.9$ (c) $d/k = 2.6$; (d) $d/k = 3.2$; (e) $d/k = 4.1$; and (f) $d/k = 5.9$. A lateral position y of 0 mm denotes the centreline of the flume and the streamwise position x relates to the position in the DEM of the bed (Figure 7a). Flow is from left to right. Note that this figure should be viewed in colour.

22

Figure 4. The spatial distribution of $\bar{u}/\langle\bar{u}\rangle$ over the bimodal bed for the experimental runs performed at a single bed slope with (a) $d/k = 1.3$; (b) $d/k = 2.0$; (c) $d/k = 2.7$; (d) $d/k = 3.3$; (e) $d/k = 4.3$; and (f) $d/k = 6.2$. A lateral position y of 0 mm denotes the centreline of the flume and the streamwise position x relates to the position in the DEM of the bed (Figure 7b). Flow is from left to right. Note that this figure should be viewed in colour.
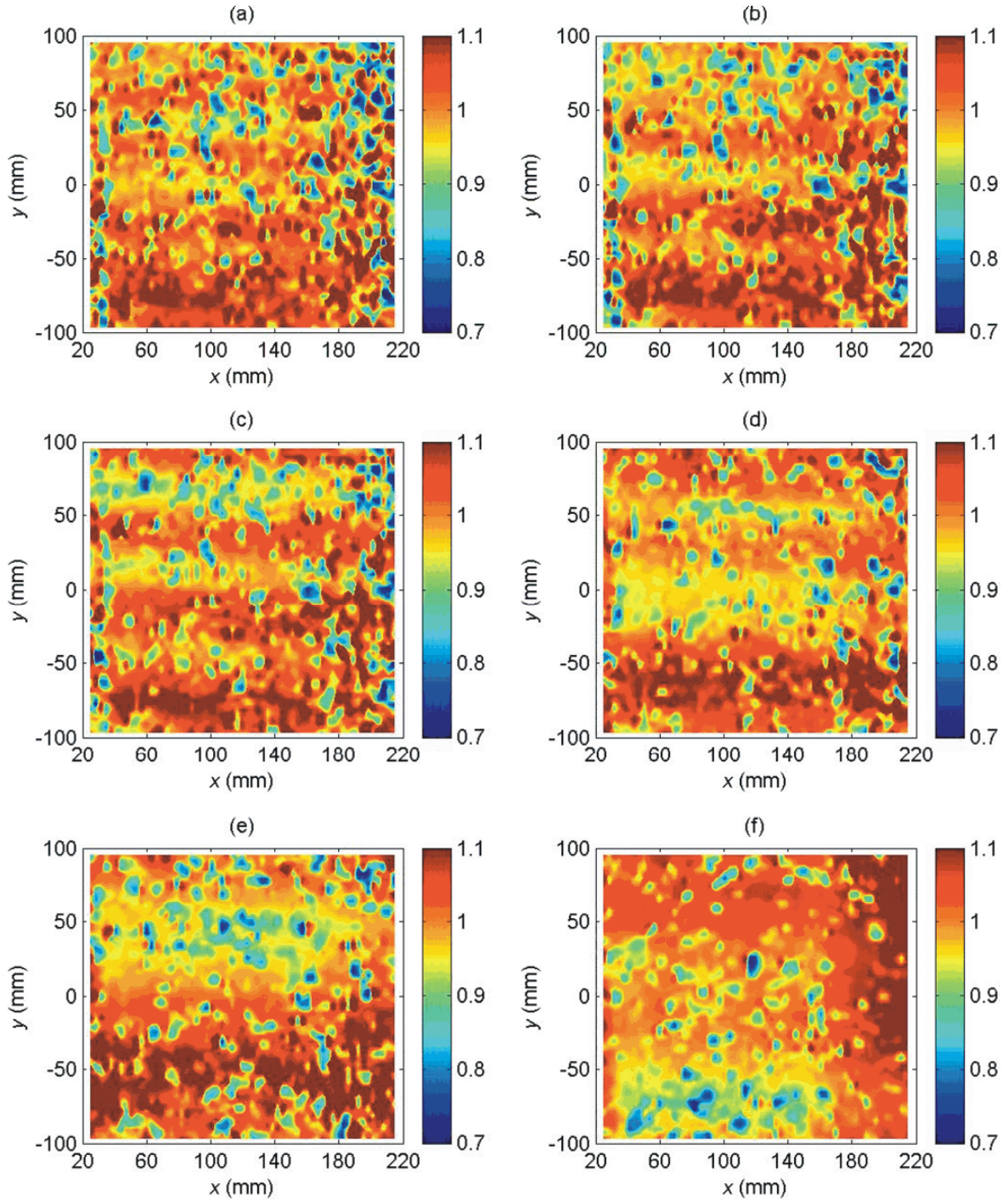
Figure 5. The spatial distribution of $\bar{u}/\langle\bar{u}\rangle$ over the unimodal bed for the experimental runs performed at the same mean bed shear stress with (a) $d/k = 1.9$; (b) $d/k = 2.2$ (c) $d/k = 2.6$; (d) $d/k = 3.2$; (e) $d/k = 4.2$; and (f) $d/k = 5.9$. A lateral position y of 0 mm denotes the centreline of the flume and the streamwise position x relates to the position in the DEM of the bed (Figure 7a). Flow is from left to right. Note that this figure should be viewed in colour.

Figure 6. The spatial distribution of $\bar{u}/\langle\bar{u}\rangle$ over the bimodal bed for the experimental runs performed at the same mean bed shear stress with (a) $d/k = 2.0$; (b) $d/k = 2.3$ (c) $d/k = 2.7$; (d) $d/k = 3.4$; (e) $d/k = 4.3$; and (f) $d/k = 6.2$. A lateral position y of 0 mm denotes the centreline of the flume and the streamwise position x relates to the position in the DEM of the bed (Figure 7b). Flow is from left to right. Note that this figure should be viewed in colour.

25
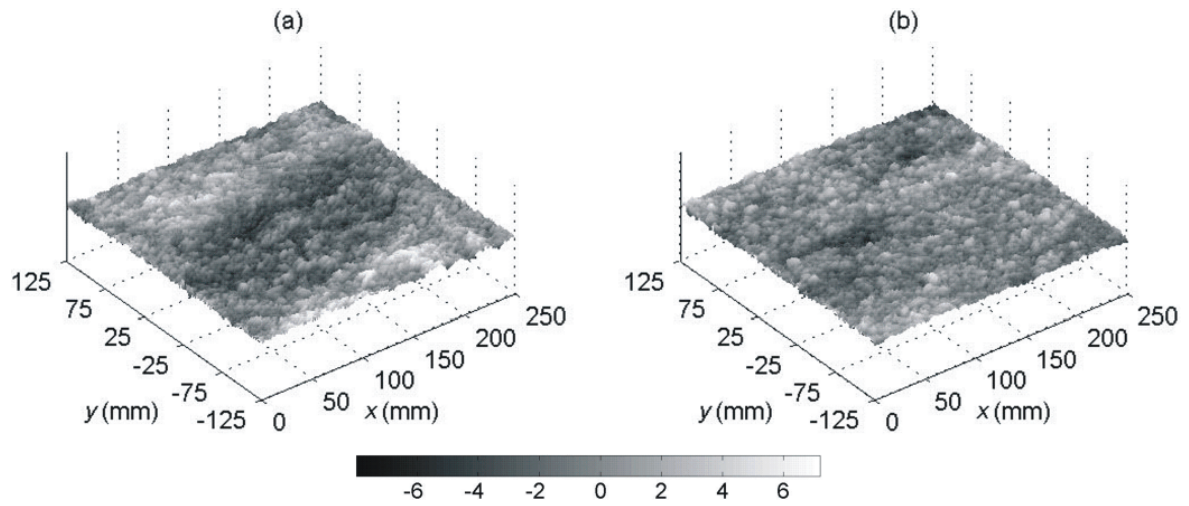
Figure 7. Digital Elevation Models of the bed surface topography of (a) the unimodal bed; and (b) the bimodal bed produced by a laser bed scanner. The grayscale relates to the departure in elevation from the zero mean surface elevation (mm). A lateral position y of 0 mm denotes the centreline of the flume and the increasing values in the streamwise position x are in the direction of the flow.
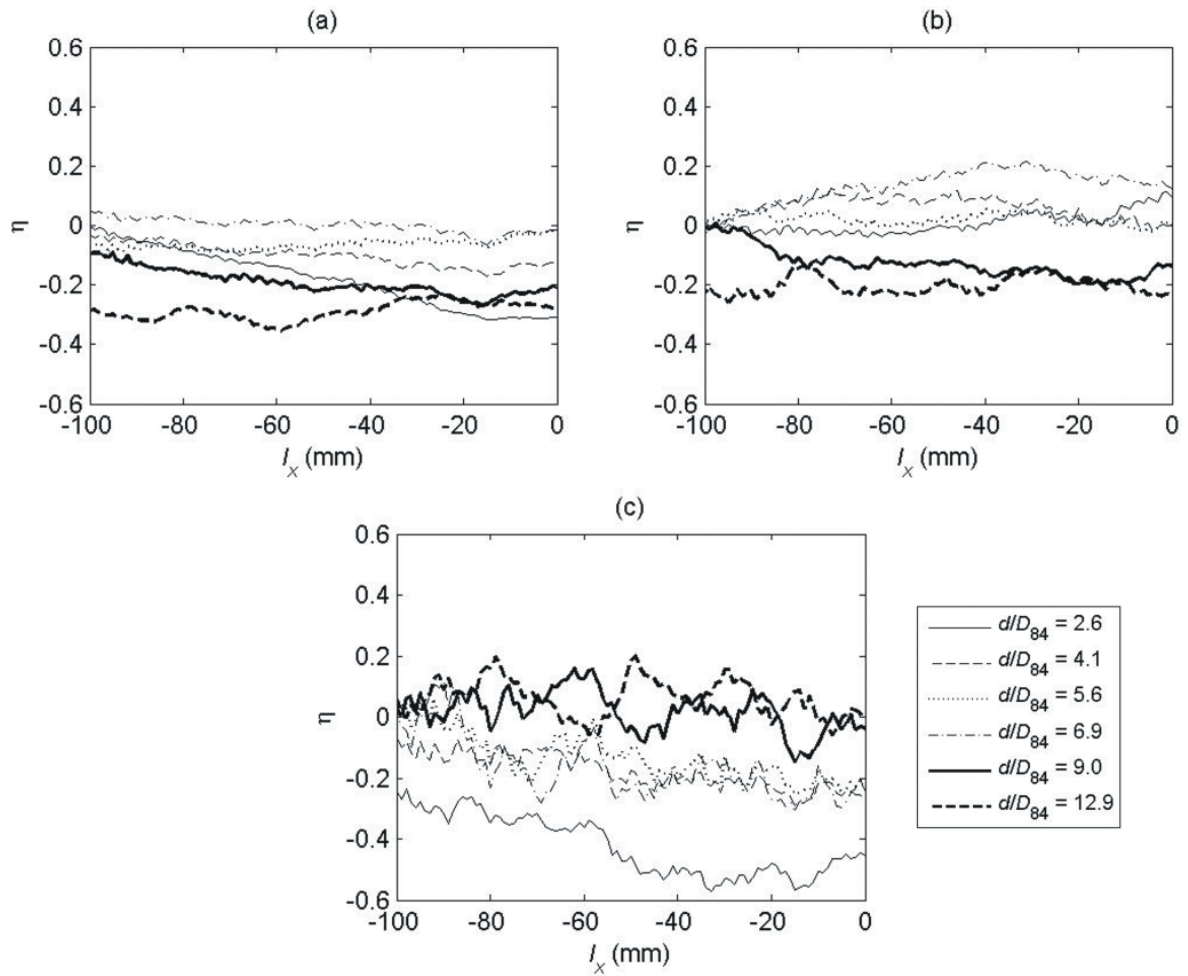
Figure 8. The coefficient of cross-correlation η with streamwise lag l_x between (a) $\bar{u}/\langle\bar{u}\rangle$ and bed surface elevation; (b) $\bar{u}/\langle\bar{u}\rangle > 1$ and bed surface elevation; and (c) $\bar{u}/\langle\bar{u}\rangle < 0.9$ and bed surface elevation, for the experimental runs carried out at a single bed slope over the unimodal bed.
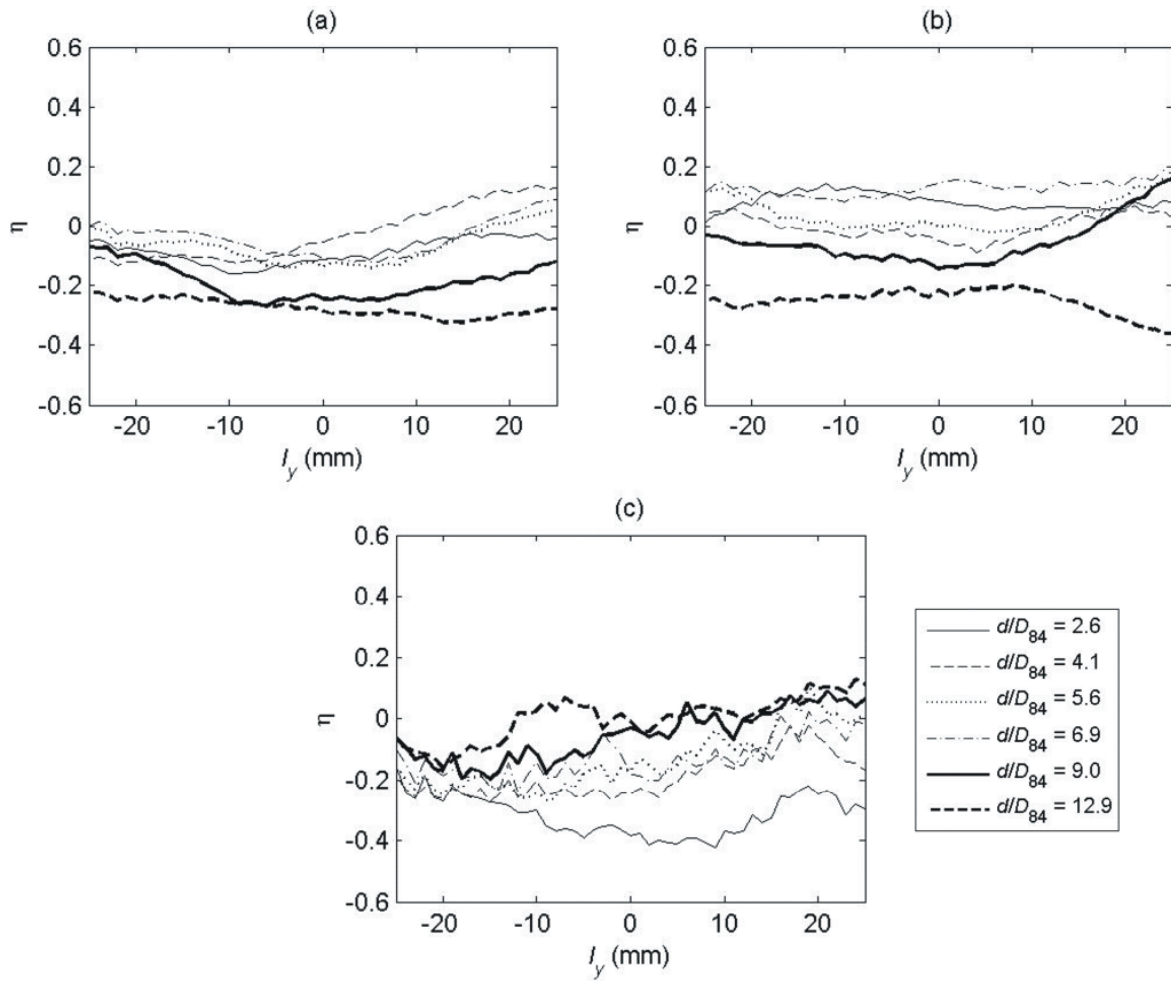
Figure 9. The coefficient of cross-correlation η with lateral lag l_y between (a) $\bar{u}/\langle\bar{u}\rangle$ and bed surface elevation; (b) $\bar{u}/\langle\bar{u}\rangle > 1$ and bed surface elevation; and (c) $\bar{u}/\langle\bar{u}\rangle < 0.9$ and bed surface elevation, for the experimental runs carried out at a single bed slope over the unimodal bed.
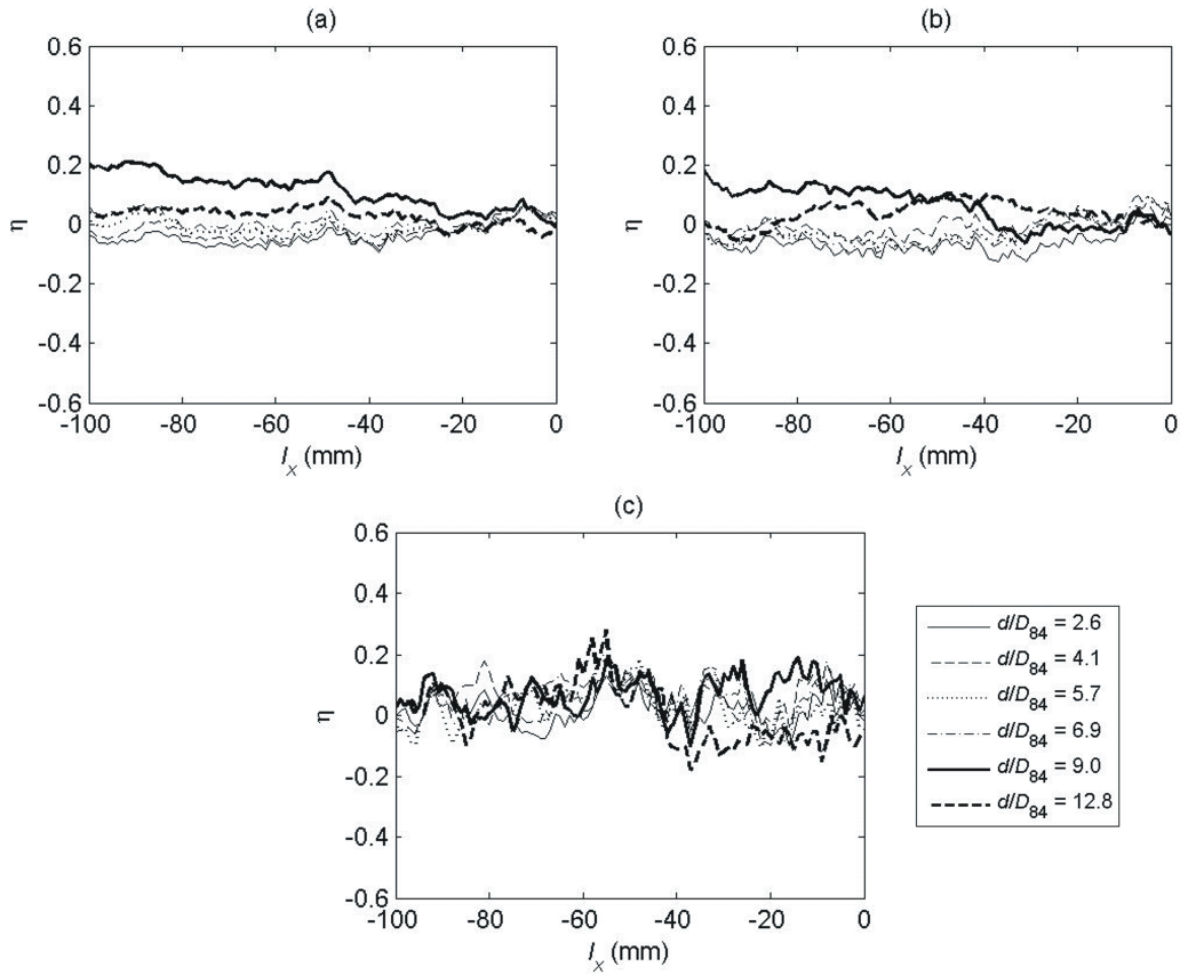
Figure 10. The coefficient of cross-correlation η with streamwise lag l_x between (a) $\overline{u}/\langle\overline{u}\rangle$ and bed surface elevation; (b) $\overline{u}/\langle\overline{u}\rangle > 1$ and bed surface elevation; and (c) $\overline{u}/\langle\overline{u}\rangle < 0.9$ and bed surface elevation, for the experimental runs carried out at a single bed slope over the bimodal bed.

Figure 11. The coefficient of cross-correlation η with lateral lag l_y between (a) $\bar{u}/\langle\bar{u}\rangle$ and bed surface elevation; (b) $\bar{u}/\langle\bar{u}\rangle > 1$ and bed surface elevation; and (c) $\bar{u}/\langle\bar{u}\rangle < 0.9$ and bed surface elevation, for the experimental runs carried out 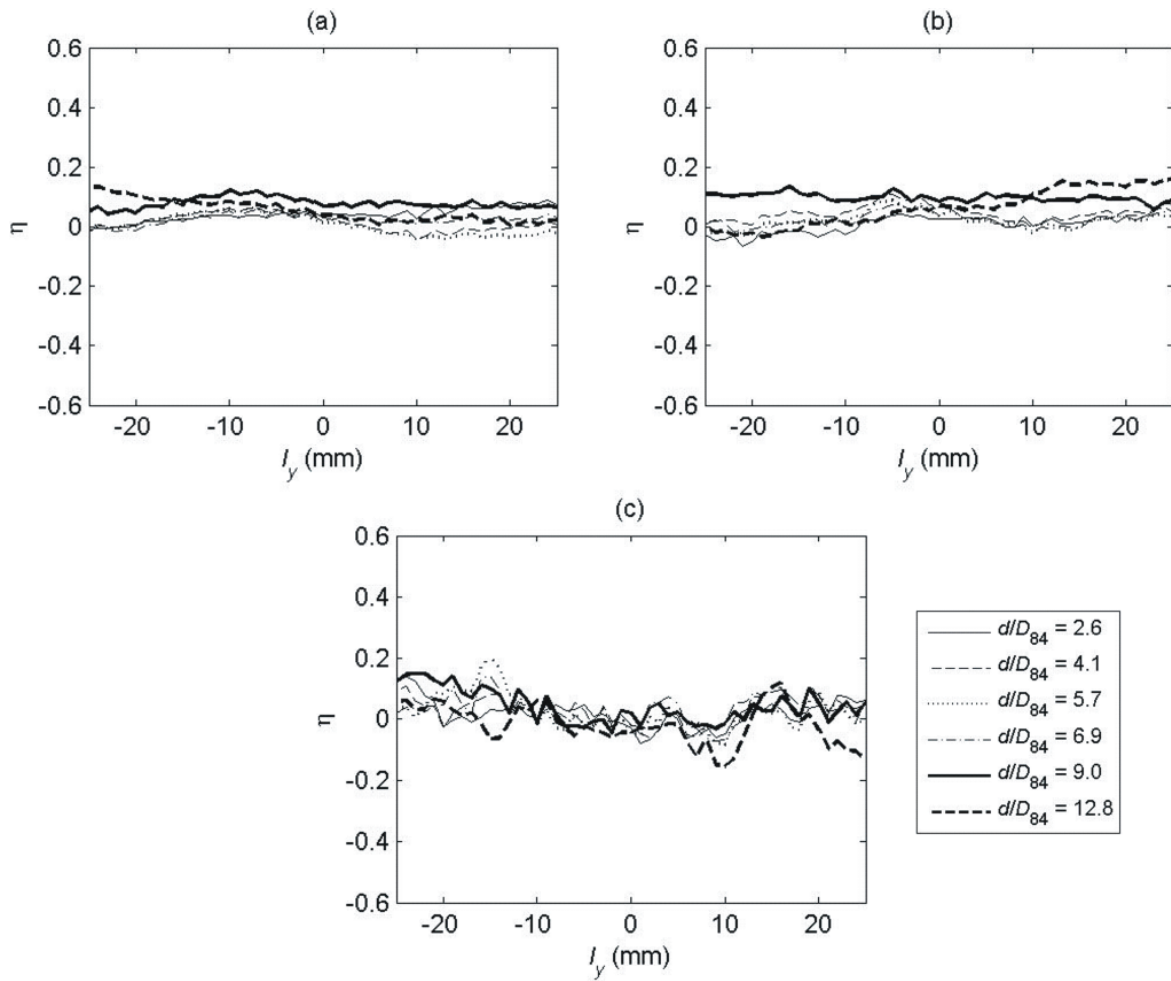at a single bed slope over the bimodal bed.